Journal of Catalysis **184,** 5–18 (1999)
Article ID jcat.1999.2392, available online at http://www.idealibrary.com on IDEAL®

Chromia–Vanadia Catalysts Supported on TiO_2: Effect of Composition on the Physicochemical Properties and Catalytic Performance for the Selective Catalytic Reduction of NO with NH_3

Ch. Fountzoula,*,† H. K. Matralis,† Ch. Papadopoulou,*,† G. A. Voyiatzis,† and Ch. Kordulis*,†,[1]

*Department of Chemistry, University of Patras, GR. 265 00, Patras, Greece; and †Institute of Chemical Engineering and High Temperature Chemical Processes, (ICE/HT-FORTH), P.O. Box 1414, GR. 265 00, Patras, Greece

Received December 8, 1997; revised December 7, 1998; accepted December 10, 1998

Chromia–vanadia on titania catalysts containing 8 mol% (Cr + V) were prepared and tested for the selective catalytic reduction (SCR) of NO by NH_3, in excess O_2, in the temperature range 250–450°C. The physicochemical properties of the prepared catalysts as well as those of the corresponding single active phase-containing samples were investigated by specific surface area and pore volume measurements, X-ray powder analysis, UV–visible diffuse reflectance spectroscopy, laser-Raman microscopy, X-ray photoelectron spectroscopy, analytical electron microscopy, and temperature-programmed reduction experiments. The best catalytic performance was achieved by the catalyst containing 2 mol% Cr and 6 mol% V ($TiCr_2V_6$), while all the binary active phase-containing catalysts proved to be more active than the corresponding single active phase-containing catalysts, at reaction temperatures higher than 350°C. The enhanced catalytic performance of the binary active phase-containing catalysts is attributed to a synergy developed between the two active phases. This synergy is maximized in the $TiCr_2V_6$ sample, where a new Raman band, at 971 cm^{-1}, has also been observed. This peak is attributed to isolated Cr^{6+} species decorated by well-dispersed V^{5+} species. Deposition of the chromia phase on the titania surface stabilizes the texture of the final catalysts against changes provoked by deposition of the vanadia phase.

Key Words: **chromia–vanadia catalysts; selective catalytic reduction; NO; titania; synergy; X-ray photoelectron spectroscopy; diffuse reflectance spectroscopy; analytical electron microscopy.**

INTRODUCTION

Environmental pollution is due largely to the emission of nitrogen oxides and sulfur oxides from synthetic sources. These oxides play a major role in the acidification of our environment.

Selective catalytic reduction (SCR) of nitrogen oxides by ammonia is among the most effective commercial methods for controlling NO_x emission from stationary sources (i.e., power stations). The most common catalysts for the SCR of nitrogen oxides used on a commercial scale are V_2O_5/TiO_2, V_2O_5–MoO_3/TiO_2, and V_2O_5–WO_3/TiO_2.

Chromium oxide catalysts unsupported or supported mainly on TiO_2 (anatase) have been extensively studied over the last decade for the SCR of NO with NH_3 in the presence of excess oxygen by the groups of Baiker and of Curry-Hyde (1–13). They have proved that chromium oxide-based catalysts containing amorphous chromia as the active phase are quite promising catalysts for low-temperature SCR operations. The selectivity toward N_2 of these catalysts in the low reaction temperature range has been shown to be similar to the selectivity found for state-of-the-art vanadium oxide-based catalysts (1).

At high reaction temperatures, however, where the amorphous chromia is transformed into crystalline α-Cr_2O_3, the selectivity of the above-mentioned catalysts toward N_2 has been proved to be lower than that exhibited by the vanadium oxide-based catalysts, making these catalysts unsuitable for practical applications (6, 14, 15).

In a recent work we studied the influence of chromium content on the physicochemical properties and catalytic behavior of chromia–titania catalysts for the title reaction at relatively high temperatures (16). The main conclusions drawn from this work were the following: (i) Isolated Cr^{6+} species, well interacted with the anatase surface, are stabilized even at high temperatures (500°C) for chromia–titania catalysts with low chromium content. (ii) These Cr^{6+} species exhibit enhanced catalytic performance for the SCR of NO with NH_3 at high reaction temperatures. (iii) Increases in the chromium content favor the formation of badly dispersed chromia phases with lower oxidation states.

Having in mind the very good catalytic performance of chromia-based catalysts for SCR of NO with NH_3 in the low reaction temperature range, their good behavior, even at high reaction temperatures when they contain isolated Cr^{6+} surface species, and the widely accepted high efficiency of the vanadium oxide-based catalysts for the same reaction

[1] To whom all correspondence should be addressed. Fax: (+30–61) 994 796.

0021-9517/99 $30.00

at high temperatures, we prepared and studied a series of binary active phase (CrO_3 and V_2O_5) containing catalysts supported on TiO_2.

Some years ago Wong and Nobe (17) studied the catalytic performance of the following SCR catalysts: Cr_2O_3/TiO_2, V_2O_5/TiO_2 and V_2O_5–Cr_2O_3/TiO_2. In all these catalysts the total active phase loading was 10 wt% and the ratio of vanadium to chromium oxide was 20 : 1. Their results showed that V_2O_5/TiO_2 catalysts are more active and selective than Cr_2O_3/TiO_2 catalysts, while the activity and selectivity of V_2O_5–Cr_2O_3/TiO_2 catalysts are comparable to those of V_2O_5/TiO_2 catalysts. To our knowledge, however, there has not been, up to now, any systematic study of the influence of the active phase composition on the catalytic behavior of V_2O_5–Cr_2O_3/TiO_2 catalysts. On the other hand, it is well known, in the field of catalysis, that the cooperation (synergy) of two or more active phases at certain ratios (synergistic ratios) could result in catalysts with exceptionally good catalytic performance (18).

In this work we focus on the influence of the composition of binary active phase V_2O_5–Cr_2O_3/TiO_2 catalysts on their catalytic performance and physicochemical properties.

EXPERIMENTAL

Catalyst Preparation

Anatase (Sakai, 98% TiO_2, 1% total SO_4^{2-}, 0.1% Fe, 0.1% Nb, 0.01% K_2O, and 0.01% P_2O_5) calcined at 500°C for 20 h was used for preparing the catalysts studied in this work.

Chromium was deposited on the titania surface by wet impregnation with an aqueous solution of $(NH_4)_2Cr_2O_7$. The water was removed slowly (over a 4-h period) in a rotary evaporator and the solid obtained was dried at 110°C for 5 h and then calcined at 500°C for 20 h in air.

Vanadium was deposited on an aliquot of the chromium-containing solids by wet impregnation using a vanadium oxalate aqueous solution. The above procedures were followed for the removal of water and the thermal treatment of the ternary catalysts so obtained. Another series of catalysts containing the same amount of vanadia phase with the corresponding ternary samples was prepared for comparison. The samples prepared are denoted hereafter as $TiCr_xV_y$, where x and y indicate the content of chromium and vanadium, respectively, expressed in mole percent.

Catalyst Characterization

Textural properties. Specific surface area and pore volume measurements were carried out in a Micromeritics ASAP 2000 apparatus, at −196°C using nitrogen as adsorption gas.

X-ray powder analysis (XRD). X-ray diffraction patterns were obtained in the range 15°–60° (scanning rate: 2° min^{-1}) with a Philips PW 1480 automated diffractometer using Cu$K\alpha$ ($\lambda = 1.4518$ Å) radiation filtered through Ni.

Diffuse reflectance spectroscopy (DRS). The diffuse reflectance spectra of the samples studied were recorded in the range 200–800 nm at room temperature, using a UV–vis spectrophotometer (Varian Cary 3) equipped with an integration sphere. TiO_2 carrier was used as a reference in all cases. The powder samples were mounted in a quartz cell which provided a sample thickness greater than 3 mm and guaranteed correct infinite sample thickness.

Laser-Raman microscopy (LRM). The Raman spectra were excited with the 514.5-nm line of a Spectra Physics (Model 163-A42) air-cooled Ar^+ laser. The spectral resolution was 9 cm^{-1}. A Jobin Yvon T-64000 Raman system equipped with a Spectraview-2D liquid N_2-cooled CCD detector was used, in the single spectrograph option, to disperse and detect the Raman scattered light. Details concerning operation conditions as well as the procedures used were given in our previous work (16).

X-ray photoelectron spectroscopy (XPS). The XPS analysis was performed at room temperature with a SSX-100 Model 206 Surface Science Instruments (SSI) photoelectron spectrometer, interfaced to a Hewlett–Packard 9000/310 computer. Details concerning operation and calibration conditions as well as the assumptions and routines used were given in our previous work (16).

Analytical electron microscopy (AEM). Analytical electron microscopy was performed on a Jeol Temscan 100 CX electron microscope equipped with a Kevex 5100 C energy-dispersive spectrometer for X-ray microanalysis. The samples were dispersed in water and deposited on a carbon film supported on a copper grid.

Temperature-programmed reduction (TPR). The apparatus used and the experimental details of the TPR experiments are described in detail elsewhere (19).

Catalytic tests. Catalytic tests were carried out in a continuous-flow tubular fixed-bed microreactor. The reaction mixture consisted of 800 ppm NO, 800 ppm NH_3, and 4% O_2 with a balance of nitrogen. This gas mixture was produced by mixing nitrogen (Air Liquide 99.999%) and single-component gases in a balance of nitrogen (8861 ppm NO/N_2, 1.02% NH_3/N_2, certified by ±1 and ±5%, respectively, Air Liquide). Feed and product concentrations of NO, NO_2, N_2O, NH_3, H_2O, and O_2 were quantitatively analyzed using a computer-controlled quadruple mass spectrometer (VG-Sensorlab 200D). Under our experimental conditions, NH_3 oxidation on the filament (producing NO) when O_2 was present in the feed was not observed. This was verified by comparing the signal at 17 amu in the presence and absence of O_2 in the calibration stream. To determine the NH_3 concentration, the contribution from the H_2O fragmentation to the signal at 17 amu was taken into account.

Finally, calibration of the mass spectrometer for NO_2 fragmentation was not necessary since, under our experimental conditions, NO_2 was never detected although the signal at 46 amu was continually monitored.

Quantities of 3 mg of catalyst diluted up to 100 mg with SiO_2 (Silica gel 60, Merck) were used in these measurements. An O_2/N_2 mixture containing 10% O_2 was passed through the reactor and the catalytic bed was heated in two successive steps, first from room temperature to 100°C and then from 100 to 450°C, and remained under these conditions for 45 min. Between these two steps, the temperature was maintained at 100°C also for 45 min. This time was required for the signal of 18 amu (H_2O), monitored by the mass spectrometer, to be stabilized. Then, the reaction mixture, with a flow rate of 150 ml min^{-1} (STP), was fed to the reactor and conversion measurements as a function of temperature were carried out in the range 250–450°C. Reaction steady state was established after 30–45 min at each temperature. Percentage yields to N_2 are defined as

$$\%Y_{N_2} = \frac{F_{NO,in} + F_{NH_3,in} - F_{NO,out} - F_{NH_3,out} - 2F_{N_2O,out}}{2(F_{NO,in} + F_{NH_3,in})} \times 100, \quad [1]$$

where F is the molar flow rate (mol s^{-1}) of the various reactants and products at the reactor inlet and outlet, as indicated by the corresponding subscripts. Both reactants, which were equimolarly mixed in the reaction mixture, were taken into account because of the uncertain stoichiometry of the reactions leading to N_2 and N_2O formation (3).

RESULTS

Texture

The compositions, BET specific surface areas, and pore volumes of the prepared samples are listed in Table 1.

TABLE 1

Catalysts Prepared and Their Compositions, BET Specific Surface Areas (S_{BET}), and Pore Volumes (PV)

Catalyst	V : Cr : Ti atomic ratio	Cr_2O_3 (wt%)	V_2O_5 (wt%)	S_{BET} (m^2/g)	PV (cm^3/g)
$TiCr_0V_0$	0 : 0 : 100	0.0	0.0	70	0.361
$TiCr_2V_0$	0 : 2 : 98	1.9	0.0	61	0.339
$TiCr_4V_0$	0 : 4 : 96	3.8	0.0	61	0.329
$TiCr_6V_0$	0 : 6 : 94	5.7	0.0	59	0.319
$TiCr_8V_0$	0 : 8 : 92	7.6	0.0	59	0.317
$TiCr_6V_2$	2 : 6 : 92	1.9	6.8	62	0.305
$TiCr_4V_4$	4 : 4 : 92	3.8	4.5	59	0.269
$TiCr_2V_6$	6 : 2 : 92	5.7	2.3	51	0.285
$TiCr_0V_8$	8 : 0 : 92	0.0	9.0	32	0.276
$TiCr_0V_6$	6 : 0 : 92	0.0	6.9	42	0.297
$TiCr_0V_4$	4 : 0 : 92	0.0	4.7	55	0.312
$TiCr_0V_2$	2 : 0 : 92	0.0	2.4	64	0.350

A significant decrease in the surface area and pore volume is observed in the case of the $TiCr_0V_y$ samples as the vanadium content increases. The corresponding pore size distribution curves showed that this decrease is accompanied by a progressive disappearance of the relatively narrow pores of the support (pore diameter ca. 150 Å) and a simultaneous creation of wider ones (pore diameter ca. 400 Å).

The specific surface areas of the ternary catalysts decrease with an increase in vanadium loading. However, this decrease is lower than that observed for the corresponding $TiCr_0V_y$ samples. On the other hand, there is no systematic change in the pore volume of the ternary catalysts as their composition changes.

The corresponding pore size distribution curves showed that the increase in vanadium content (and simultaneous decrease in chromium content) brought about a shift of the maxima toward larger pore diameters. However, a comparison of the corresponding curves for the $TiCr_0V_y$ and $TiCr_xV_y$ catalysts revealed that the above-mentioned shift is stronger in the absence of the chromia phase.

Structure

The X-ray diffraction patterns of the fresh $TiCr_xV_y$ catalysts exhibited only the diffraction lines of anatase. However, electron microscopy revealed the existence of well-formed crystalline phases other than that of the support phase. As the energies of the X rays emitted from the vanadia and chromia phase do not differ enough, it was not easy to perform quantitative microanalysis on the ternary samples. Electron microscopy results showed that in the $TiCr_8V_0$ sample, the chromia phase is not dispersed very well on the titania surface and some crystallites are formed. These crystallites are either free or associated with the support particles. Figure 1a shows that the chromia and vanadia phases are also ill-dispersed in the $TiCr_6V_2$ catalyst. Similarly, $TiCr_4V_4$ catalyst contains aggregates that seem more bulky than those observed in the other catalysts of this series. In some of them only V and/or Cr phases are detected by microanalysis. $TiCr_2V_6$ catalyst appears more homogeneous in the corresponding electron micrograph presented in Fig. 1b. Microanalysis results have shown a slight variation in Cr and V content from one particle to the other, while no particles containing only chromium and/or vanadium phases were detected in this sample. Finally, a remarkable heterogeneity has been found in the $TiCr_0V_8$ catalyst. In some particles of this catalyst only the vanadium phase was detected, while the rest of the sample contained aggregates of various shapes and sizes.

The UV–vis/diffuse reflectance (DR) spectra of the samples containing 8 mol% active phases are illustrated in Fig. 2. A main absorption band centered at 410–420 nm is observed in all cases. This band is typical of the transition metal oxo-species in their maximum oxidation state

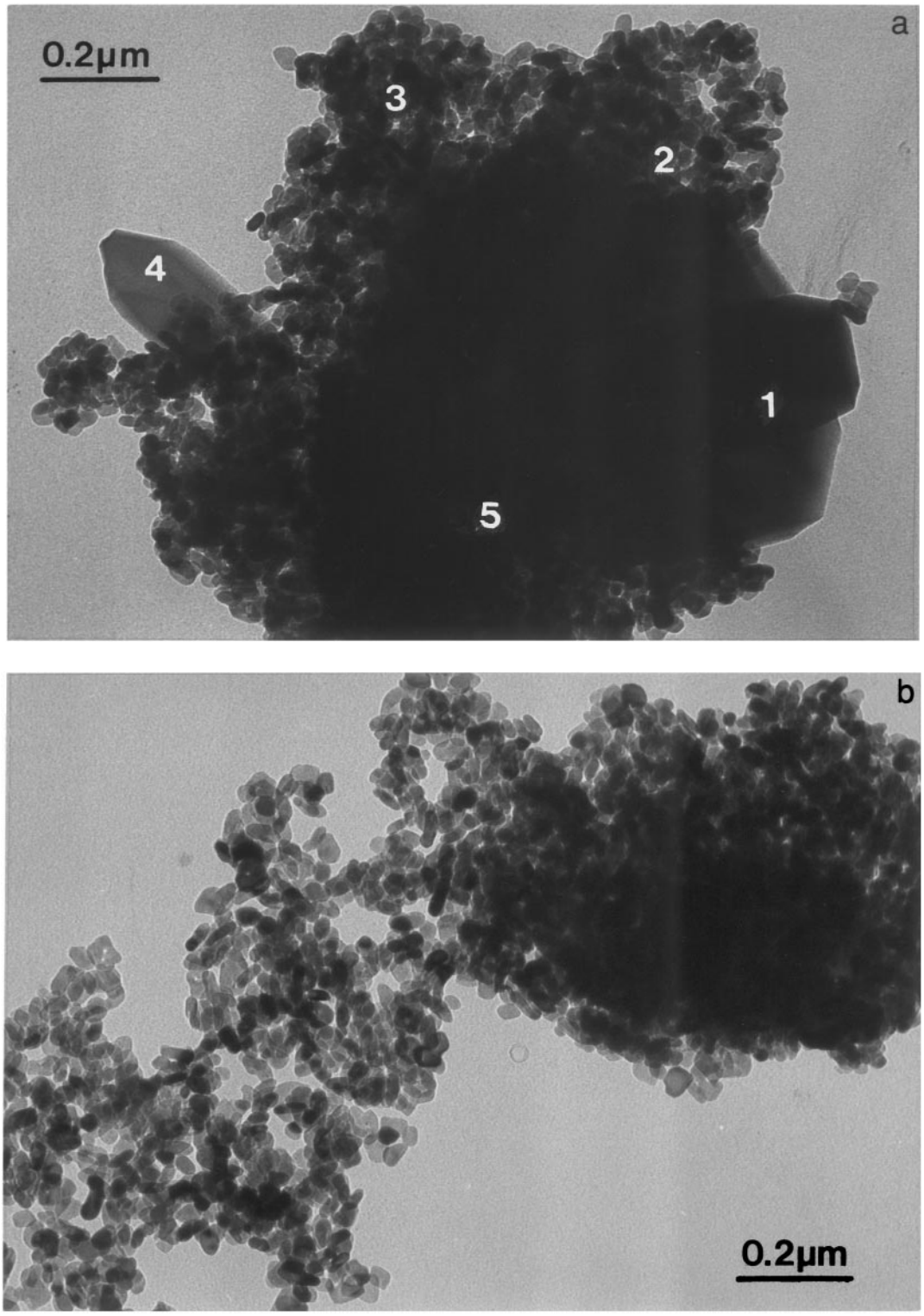

FIG. 1. (a) Electron micrograph of the $TiCr_6V_2$ sample. Elements detected: (1) Cr, (2) Ti + Cr, (3) Ti, (4) Cr, (5) Ti + Cr. (b) Electron micrograph of the $TiCr_2V_6$ sample.

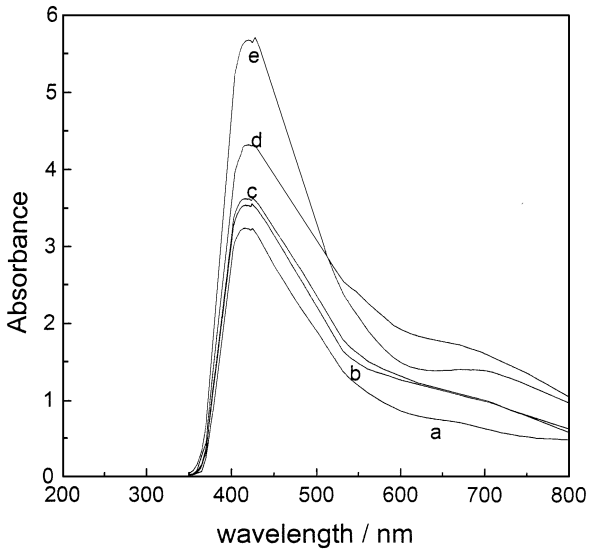

FIG. 2. UV–vis/DR spectra of the $TiCr_xV_y$ samples. (a) TiV_8, (b) $TiCr_8$, (c) $TiCr_6V_2$, (d) $TiCr_4V_4$, (e) $TiCr_2V_6$.

well interacted with the titania surface (16, 20–22). The intensity of this peak is higher in the cases of binary active phase-containing catalysts and takes its maximum value in the case of the $TiCr_2V_6$ sample. These results show that greater fractions of active species in their highest oxidation state (Cr^{6+} and V^{5+} species) are stabilized on the surface of the binary active phase-containing catalysts than on the catalysts containing a single active phase. However, it is very interesting that $TiCr_2V_6$ is the only catalyst where the intensity of the DRS band at 410–420 nm is equal to the sum of the intensities recorded in the cases of the corresponding single active phase-containing catalysts ($TiCr_2V_0$ and $TiCr_0V_6$). In all other cases the intensity of this band does not exceed an average of about 70% of the abovementioned sum.

The shape of the absorbance band for the $TiCr_0V_8$ sample (Fig. 2a) reveals contributions from absorption at 430 and 500 nm which are due to the $O^{2-} \rightarrow V^{5+}$ charge transfer process (23), indicating the presence of crystalline V_2O_5 in this sample (24). This is in agreement with our AEM results, although this phase was not detectable by XRD.

The absorbance observed all along the visible region of all DR spectra presented in this work is attributed to badly resolved absorbance bands originating from chromium- and vanadium-supported species where the corresponding metals exist at oxidation states other than their maximum (25). In the case of the Cr surface species, it is well known that Cr^{3+} species are the most abundant after calcination at 500°C (16).

Important changes in the features of the Raman spectra with the composition of the $TiCr_xV_y$ samples have been observed in the spectral region 700–1000 cm^{-1}. Figure 3 presents this region for spectra recorded using "low laser intensity." With the exception of a second-order band of anatase at ~800 cm^{-1} (26), chromium oxide and vanadium oxide phase symmetric and antisymmetric stretching modes can be obtained (7, 16, 26–31). Inspection of this figure shows that, in fact, more than one badly resolved peak appears in this region, creating a scattering envelope. Starting from the sample containing 8 mol% Cr, an increase is observed in the intensity of the envelope of the Raman bands

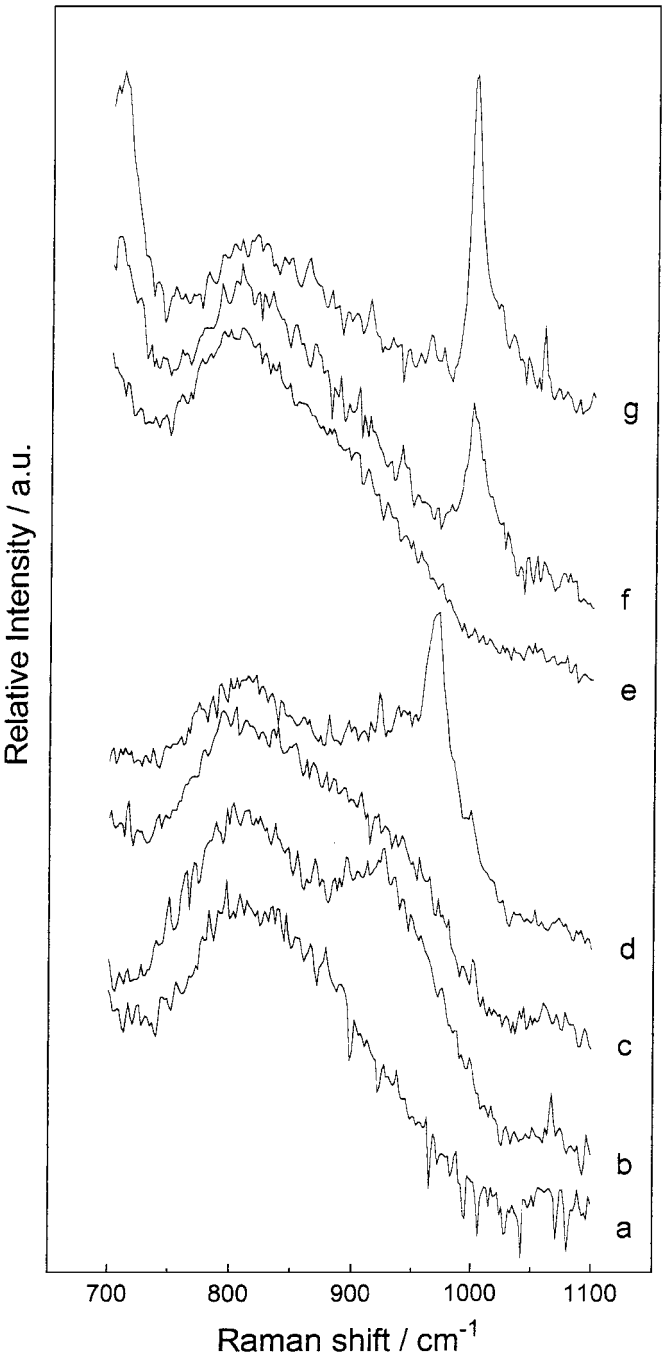

FIG. 3. Laser Raman spectra of the $TiCr_xV_y$ samples recorded using "low laser intensity." (a) $TiCr_8$, (b) $TiCr_6V_2$, (c) $TiCr_4V_4$, (d) $TiCr_2V_6$, (e) $TiCr_2$, (f) TiV_6, (g) TiV_8.

at shifts higher than 870 cm^{-1}, as the chromia phase is substituted by vanadia. A new very sharp peak appears in the spectrum of the $TiCr_2V_6$ sample at 971 cm^{-1}, superimposed on the above-mentioned envelope, accompanied by a small peak at 997 cm^{-1}, which is characteristic of pure crystalline V_2O_5 (28, 29). Finally, in the case of the $TiCr_0V_8$ sample, under the experimental conditions used, only the second-order band of anatase at ~800 cm^{-1} and the sharp peak at 997 cm^{-1} appear clearly. The last peak, in agreement with the DRS and AEM results, verifies the formation of crystalline V_2O_5 on the surface of the $TiCr_0V_8$ sample.

Laser-induced changes in chromia or vanadia supported on titania samples have been reported by several authors (7, 16, 32). More precisely, it is well established that crystallization of the chromia phase takes place when a chromia–titania sample is irradiated by a laser beam with "high laser intensity." On the other hand, exposure of a vanadia–titania catalyst to increasing laser power is accompanied by a decrease in the intensity of the band near 995 cm^{-1} and a simultaneous increase in the band at 1030 cm^{-1}. This behavior has been interpreted as due to dehydration of the supported vanadyl species (28–32).

The LRM spectra of the binary active phase-containing catalysts recorded using "high laser intensity" are presented in Fig. 4. Comparison of these spectra with the corresponding spectra presented in Fig. 3 shows remarkable differences in the shape of the Raman bands of the catalysts studied. However, the increase in the intensity of the Raman scattering at shifts higher than 870 cm^{-1}, which is observed as the chromia phase is substituted by vanadia in the case of the spectra recorded using "low laser intensity," is also observed in the spectra recorded using "high laser intensity." It might be noted that the relative intensity of the sharp peak observed previously at ~971 cm^{-1} in the case of the $TiCr_2V_6$ specimen was diminished after irradiation with "high laser intensity."

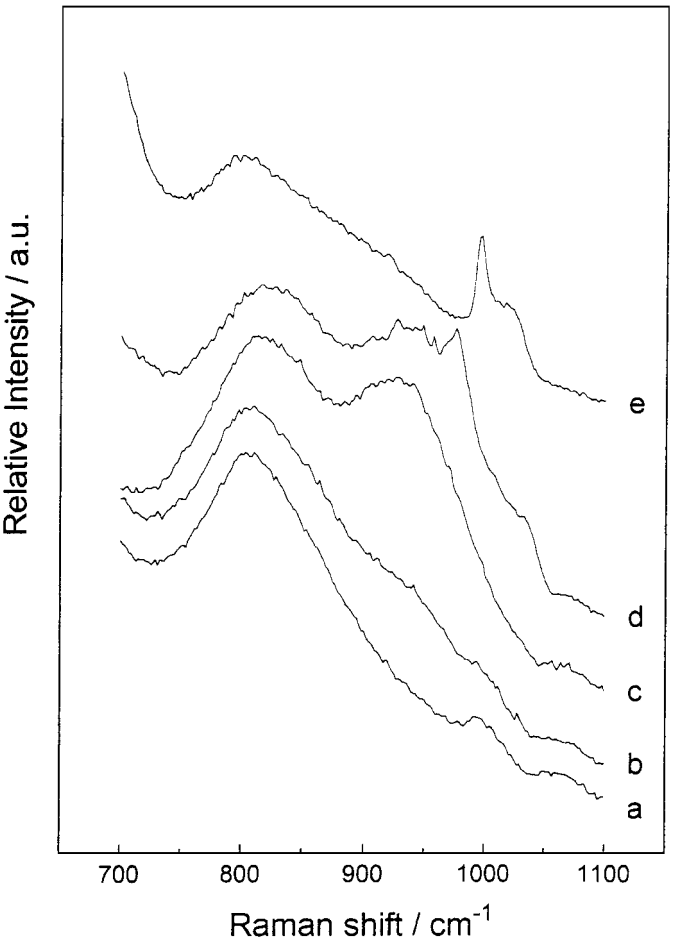

FIG. 4. Laser Raman spectra of the $TiCr_xV_y$ samples recorded using "high laser intensity." (a) $TiCr_8$, (b) $TiCr_6V_2$, (c) $TiCr_4V_4$, (d) $TiCr_2V_6$, (e) TiV_8.

Surface Properties

For all samples, the binding energies (BEs) of the O 1*s* and Ti $2p_{3/2}$ photoelectrons was, respectively, 529.8 ± 0.1 and 458.6 ± 0.1 eV.

The X-ray photoelectron spectra of the Cr 2*p* doublet of the $TiCr_xV_y$ catalysts are presented in Fig. 5. The shape of this peak definitely indicates the existence of chromium in at least two valence states, namely, Cr^{3+} concluded from the maximum at binding energy (BE) 576.9 eV, which corresponds to the photoelectrons emitted from the Cr $2p_{3/2}$ level of Cr^{3+} atoms, and Cr^{6+} concluded from the second maximum observed at BE = 579 eV. The presence of some amount of Cr^{5+} [BE(Cr $2p_{3/2}$) = 577.5–578.5 eV] cannot be excluded, taking into account the shape of these spectra. Unfortunately, no information could be obtained from the X-ray photoelectron spectra of these catalysts concerning the existence of Cr^{4+} species on the TiO_2 surface. The electrons of the 2*p* level in these species have a binding energy too close to that of Cr^{3+} species and exhibit the same multiple splitting but a somewhat larger peak width (26, 27).

Although in principle a deconvolution of the Cr $2p_{3/2}$ peak of the spectra could result in a quantification of the relative concentrations of the above-mentioned species, this has not been attempted. The main reason is the well-known fact that under XPS analysis conditions part of Cr^{6+} is reduced to lower-oxidation-state species (28). We have verified this by long-time analysis in the X-ray photoelectron spectrometer (16). However, in a first semiquantitative approximation comparing the spectra of the $TiCr_xV_y$ samples with those of the $TiCr_x$ samples with the same Cr loading we can conclude that addition of the vanadia phase decreases the concentration of Cr^{6+} species or facilitates their reduction during XPS analysis. A typical example is depicted in Fig. 6.

The BEs of V $2p_{3/2}$ photoelectrons for V^{5+} and V^{4+} species are reported to be equal to 517.0 ± 0.2 and

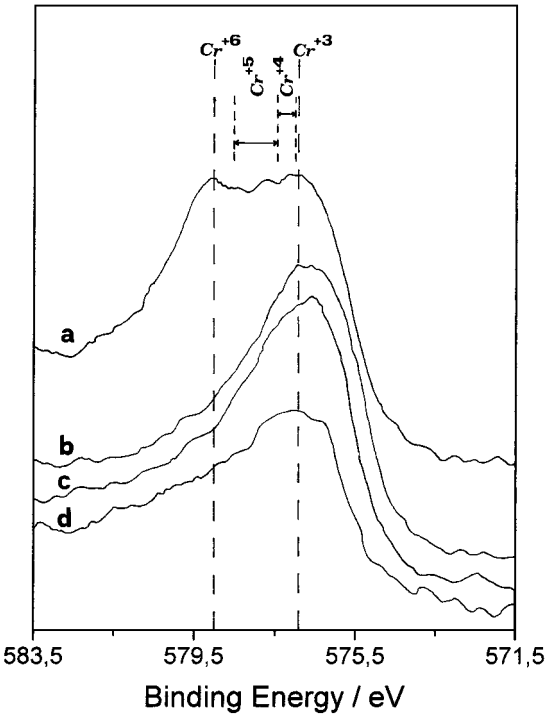

FIG. 5. X-ray photoelectron spectra of the Cr 2*p* doublet of the $TiCr_xV_y$ catalysts. (a) $TiCr_8$, (b) $TiCr_6V_2$, (c) $TiCr_4V_4$, (d) $TiCr_2V_6$.

515.9 ± 0.2 eV, respectively (33–36). In our spectra the corresponding peak appeared at 517 ± 0.2 eV, indicating the existence of V^{5+} species on the catalyst surface. However, an asymmetry toward the low binding energy side has been

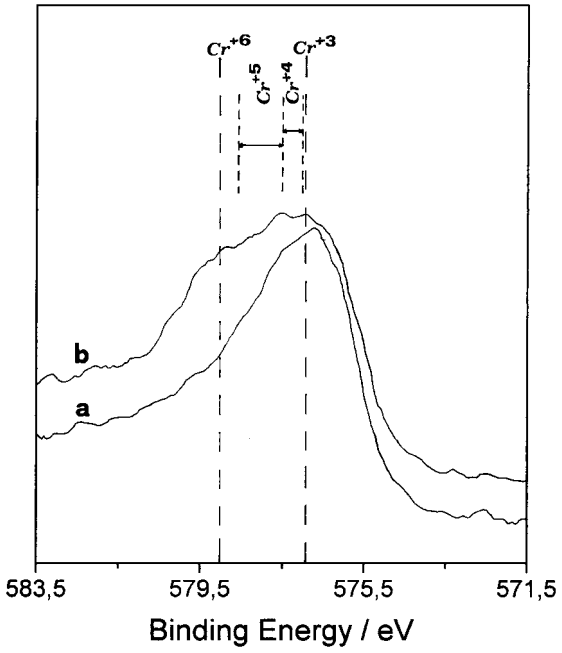

FIG. 6. X-ray photoelectron spectra of the Cr 2*p* doublet of the (a) $TiCr_4V_4$ and (b) $TiCr_4$ catalysts.

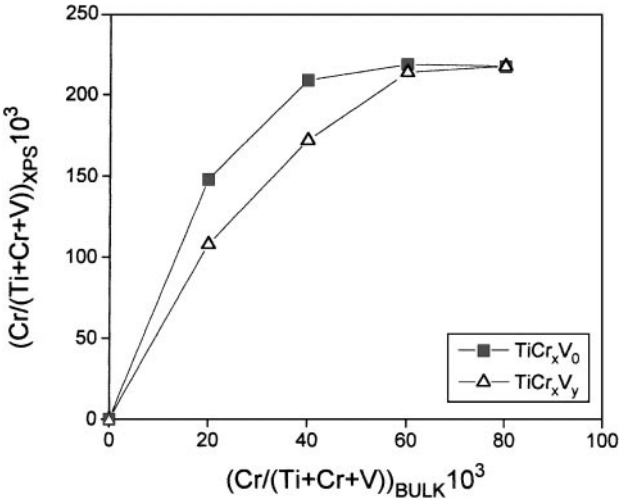

FIG. 7. Variation of the XPS surface atomic ratios $(Cr/(Ti + Cr + V))_{XPS}$ versus the corresponding bulk ratios for the $TiCr_xV_y$ and $TiCr_xV_0$ samples.

observed in the above peak in the spectra of $TiCr_2V_6$ and $TiCr_0V_8$ samples, indicating the formation in these samples of small amounts of vanadium species at a lower oxidation state, most probably V^{4+} in agreement with other results (37–40).

The variation of the XPS surface atomic ratios $(Cr/(Ti + Cr + V))_{XPS}$ versus the corresponding bulk ratios for the $TiCr_xV_y$ and $TiCr_xV_0$ samples is presented in Fig. 7. Concerning the ternary samples, it can be seen that, after an initial nonlinear increase, the coverage of TiO_2 by supported chromium species reaches its maximum at a loading equal to 6 mol% Cr ($TiCr_6V_2$) and remains constant with a further increase in Cr loading.

Comparing the values of the above-mentioned XPS surface atomic ratios measured on the $TiCr_xV_y$ samples with those measured on the $TiCr_xV_0$ samples with the same Cr loading, it is evident that deposition of the vanadia phase reduces the dispersion of the previously supported chromia phase. This sintering of the chromia phase is in agreement with the diminution in the Cr^{6+} surface species observed after deposition of the vanadia phase (Fig. 6), as it is well known that crystallization of the chromia phase produces α-Cr_2O_3.

The variation of the XPS surface atomic ratios $(V/Ti + Cr + V))_{XPS}$ versus the corresponding bulk ratios for the ternary ($TiCr_xV_y$) and binary ($TiCr_0V_y$) samples is presented in Fig. 8. Inspection of this figure shows that the surface concentration of vanadium in the ternary vanadium-poor (and thus chromium-rich) samples ($TiCr_6V_2$ and $TiCr_4V_4$) is lower than that measured on the surface of the corresponding binary samples ($TiCr_0V_2$ and $TiCr_0V_4$). This indicates that deposition of vanadium onto a CrO_x/TiO_2 catalyst with Cr_2O_3 loading in the range 4–6 mol% Cr results in a poorer vanadia dispersion, in comparison with

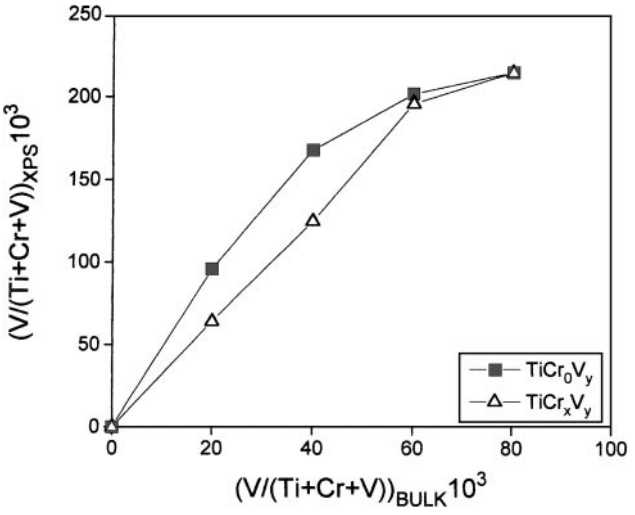

FIG. 8. Variation of the XPS surface atomic ratios $(V/(Ti + Cr + V))_{XPS}$ versus the corresponding bulk ratios for the $TiCr_xV_y$ and $TiCr_0V_y$ samples.

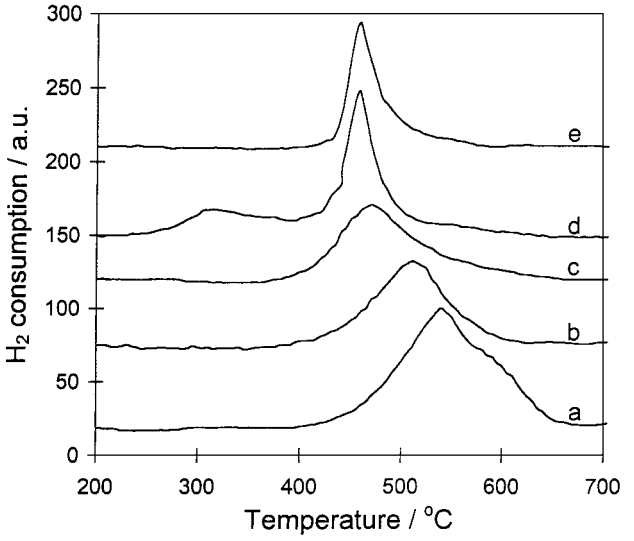

FIG. 10. TPR curves of the $TiCr_xV_y$ samples. (a) TiV_8, (b) $TiCr_2V_6$, (c) $TiCr_4V_4$, (d) $TiCr_6V_2$, (e) $TiCr_8$.

the binary $TiCr_0V_y$ system. It seems, from Fig. 8, that this is not the case for the $TiCr_2V_6$ sample.

The total surface concentrations of both supported elements expressed as the XPS atomic ratio $[(Cr + V)/(Cr + V + Ti)]_{XPS}$ are presented in Fig. 9 versus the bulk composition of the $TiCr_xV_y$ samples. This XPS atomic ratio becomes a maximum in the case of the $TiCr_2V_6$ sample, showing that the highest coverage of the support by the supported phases is achieved in this composition. In addition, one could note that all the binary active phase-containing samples exhibit higher surface coverages than the single active phase-containing samples.

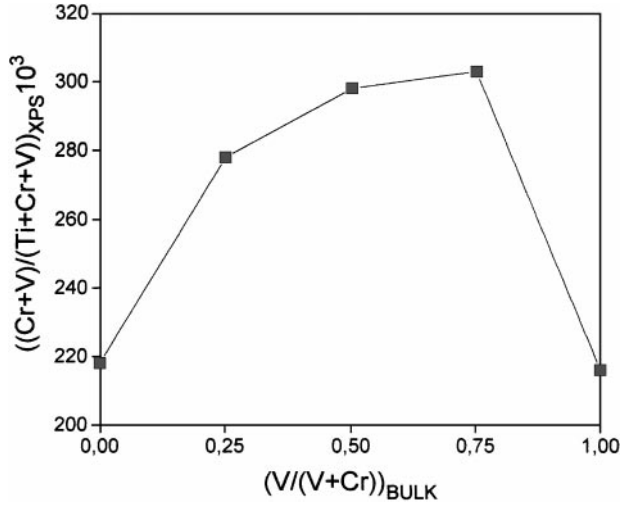

FIG. 9. Variation of the total surface concentration of both supported elements, expressed as the XPS atomic ratio $((Cr + V)/(Cr + V + Ti))_{XPS}$, versus the bulk composition of the $TiCr_xV_y$ samples.

Reactivity

The reduction behavior of binary chromia–titania and vanadia–titania catalysts has been extensively studied (6, 16, 24, 27, 41–47). Figure 10 illustrates the TPR curves of the $TiCr_xV_y$ specimens containing 8 mol% active components. It can be observed that the shape of the TPR curves changes significantly with the composition of these samples.

Catalytic Activity

The $TiCr_xV_y$ samples were very active. Conversions in the range 5–10% were achieved only at 250°C. So, we could consider our reactor working in a differential mode, and calculate specific activities, only for that reaction temperature, using the equation

$$R = \frac{F \cdot x}{\mathrm{SSA} \cdot w}, \qquad [2]$$

where F is the molar flow rate of NO or NH_3, x is the corresponding conversion, SSA is the specific surface area, and w is the weight of the sample in the reactor.

The calculated values of the specific activities (R_{NO} and R_{NH_3}) of the catalysts are presented in Table 2. The values

TABLE 2

Catalysts Prepared and Their Specific Activities, R, at $\theta = 250°C$

Catalyst	R_{NO} (μmol m^{-2} min^{-1})	R_{NH_3} (μmol m^{-2} min^{-1})
$TiCr_8V_0$	2.9	3.1
$TiCr_6V_2$	2.5	2.4
$TiCr_4V_4$	4.9	4.7
$TiCr_2V_6$	9.0	8.6
$TiCr_0V_8$	10.5	10.3

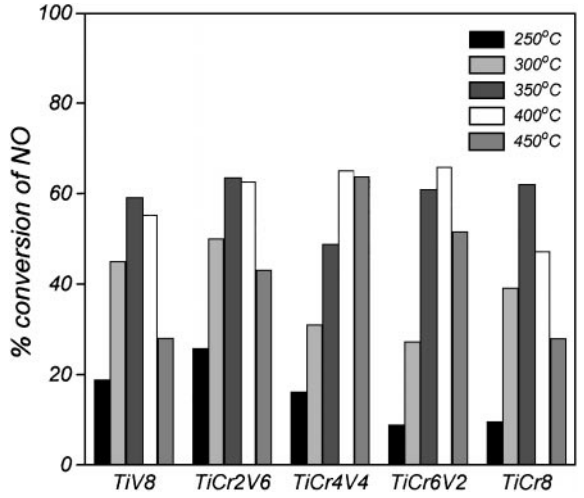

FIG. 11. Activity results, expressed as percentage NO conversion, for the $TiCr_xV_y$ samples.

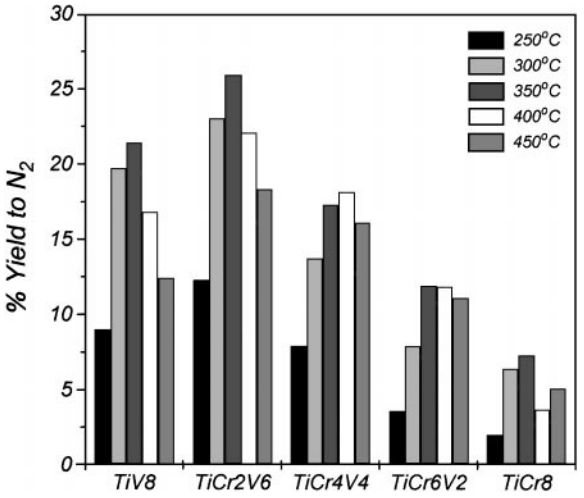

FIG. 13. Yields to N_2 obtained for the $TiCr_xV_y$ samples.

of the two specific rates almost coincide for all catalysts studied. This means that, in accordance with the literature (48–50), at this low reaction temperature the main reaction taking place during the SCR process is

$$4NO + 4NH_3 + O_2 \rightarrow 4N_2 + 6H_2O. \quad [3]$$

The specific activity increases with V content, although the global activity (activity per gram of catalyst), a measure of which is the percentage x_{NO} (Fig. 11), seems to vary with the composition of the catalysts in a different way. Indeed, at low reaction temperatures ($\leq$350°C) the catalyst containing 2 mol% Cr and 6 mol% V ($TiCr_2V_6$) proved to be the most active catalyst of this series. At high reaction temperatures ($\geq$400°C) all the ternary catalysts ($TiCr_2V_6$, $TiCr_4V_4$, and $TiCr_6V_2$) proved to be more effective than the binary ones ($TiCr_8V_0$ and $TiCr_0V_8$).

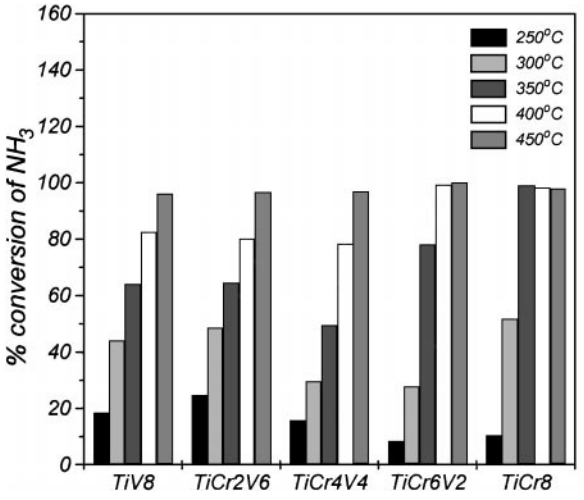

FIG. 12. Percentage NH_3 conversion for the $TiCr_xV_y$ samples.

The conversion of ammonia during the NO reduction tests is illustrated in Fig. 12. Comparison of the values for NH_3 conversion with the corresponding values for NO conversion (Fig. 11) at low reaction temperatures ($\leq$350°C) shows that ammonia consumption over the vanadium-rich catalysts ($TiCr_0V_8$, $TiCr_2V_6$, $TiCr_4V_4$) is almost stoichiometric. In the case of chromium-rich catalyst the ammonia consumption exceeded that of the NO at 350°C. This behavior is also observed at high reaction temperatures ($\geq$400°C) for all catalysts studied.

Yields to nitrogen are presented in Fig. 13. At all reaction temperatures studied, the yield to N_2 increased with V content of the catalysts up to the $TiCr_2V_6$ sample and decreased again for the $TiCr_0V_8$ sample. On the other hand, the yield to N_2 achieved for each of these catalysts increased with reaction temperature up to 350–400°C and then decreased with a further increase in reaction temperature.

DISCUSSION

Influence of Catalyst Composition on Textural Properties

In a previous work (16), we found that deposition of chromia on the anatase surface has only a slight influence on its textural characteristics. The results presented in this work show that addition of progressively higher loadings of vanadium in the $TiCr_0V_y$ samples destroyed the textural characteristics, in perfect agreement with the results of del Arco *et al.* (51).

The fact that the addition of progressively higher vanadium loadings on chromium-containing solids to prepare the ternary catalysts brought about a relatively lower decrease in the specific surface area of the samples and a weaker influence of the shape of their pore size distribution curves shows that the chromia phase has a texture

stabilizing action against the changes provoked by deposition of the vanadia phase.

Supported Species on the Surface of $TiCr_xV_y$ Catalysts

The joint use of a variety of characterization methods proved to be necessary because of the complexity of these catalysts. So, although the formation of crystalline phases like V_2O_5 and Cr_2O_3 has not been detected by XRD analysis, their existence, in addition to that of well-dispersed chromium, vanadium, and/or chromium–vanadium oxo-species, on the surface of the $TiCr_xV_y$ catalysts has been proved from the results of AEM, DRS, LRM, and XPS.

Based on the DRS results and considering that in the $TiCr_2V_0$ and $TiCr_0V_2$ samples, because of the low active phase loading, a negligible fraction is crystallized, one can calculate the values of the Kubelka–Munk function (R_∞) per mole percent of these species from the corresponding DR spectra in the range 410–420 nm. Such a calculation gave values of R_∞/mol% of $V = 0.8$ and R_∞/mol% of $Cr = 1.0$. Taking into account that these values are so close to each other, we can consider, in a first approximation, that any change in the value of R_∞ in the above-mentioned spectral region with the composition of the $TiCr_xV_y$ catalysts is not due to variation in the relative concentrations of vanadium and chromium, but reflects an analogous change in the total concentration of the chromium and vanadium oxo-species well interacted with the support surface.

Based on the above consideration, the DRS results, illustrated in Fig. 2, show that the coexistence of two active phases on the anatase surface increases the fraction of supported species that interact well with the support surface as compared with the corresponding single-active-phase catalysts with the same total loading. This fraction becomes a maximum in the case of the $TiCr_2V_6$ catalyst. This means that (i) the maximum coverage of the support surface by the supported phases should also be attained for the $TiCr_2V_6$ sample, and (ii) the coverage obtained in the ternary samples should be higher than that of the binary samples with the same total loading. Indeed, the XPS results presented in Fig. 9 strongly support both of these arguments.

As already mentioned in the results, the $TiCr_2V_6$ catalyst is the only ternary catalyst in which the value of R_∞, in the range 410–420 nm, is exactly the sum of the corresponding values, measured on the $TiCr_2V_0$ and $TiCr_0V_6$ samples. This means that the deposition of 2 mol% Cr on the support surface did not reduce the number of surface sites available for deposition of the vanadium species well interacted with the support. This picture is also corroborated by the XPS results presented in Fig. 8, in which the same value is observed for the $(V/(Ti + Cr + V))_{XPS}$ atomic ratios of the $TiCr_2V_6$ and $TiCr_0V_6$ samples. To explain this behavior one could suppose that the two phases occupy different surface sites. However, this hypothesis does not succeed in explaining the fact that in all other ternary samples the value of R_∞ in the range 410–420 nm was smaller than the 70% of the sum of the corresponding values measured on the binary samples.

Another tentative explanation, which could be proposed for the interaction of the two phases, is as follows: According to our previous work (16), isolated Cr^{6+} species of tetrahedral symmetry are mainly formed on the titania surface for chromium loading ca. 2 mol% Cr. When the chromium loading increases, oligomeric (namely, trimeric and tetrameric) species of octahedral symmetry are detected. Thus one could speculate that during the second impregnation step for deposition of the vanadia phase, hydrolysis of Ti–O–Cr bonds could take place to some extent according the following or analogous paths:

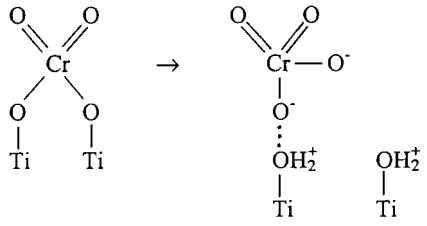

[4]

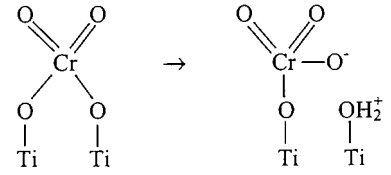

[5]

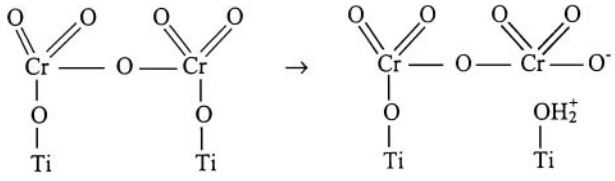

[6]

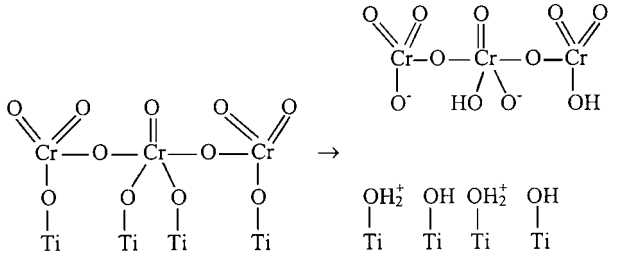

[7]

According to paths [4], [5], and [6] a large fraction of the hydrolyzed monomeric and dimeric Cr^{6+} species remains associated with the titania surface. This is in agreement with the previous findings of our group (52), namely, that the deposition of the chromia phase on the surface of TiO_2 during impregnation takes place via CrO_4^{2-}, $HCrO_4^-$, and $Cr_2O_7^{2-}$ species that are deposited on sites created by the protonated or undissociated surface hydroxyl groups of

TiO_2. In addition, it was concluded in that work that a single surface hydroxyl group is needed for deposition of each of the above Cr-containing species. According to the above hydrolysis paths, the hydrolyzed monomeric Cr^{6+} species remaining associated with the surface create a new adjacent protonated surface hydroxyl group per chromate unit. In contrast to that, fully hydrolyzed oligomeric Cr^{6+} species (path [7]) are not expected to remain associated with the support surface (53). Finally, the partially hydrolyzed oligomeric Cr^{6+} species are expected to create smaller amounts of protonated hydroxyls per chromate unit than the isolated ones, as it is induced by the hydrolyzation path (6). If our speculation is correct, namely, if the situation in the "solid/impregnating solution" interface during the impregnation of V on the $TiCr_x$ samples is like that described above, it is expected that, in the case of $TiCr_2V_6$ sample, a portion of $V_xO_y^{z-}$ species would be adsorbed on the new protonated surface hydroxyl groups formed in the vicinity of the hydrolyzed isolated chromate units remaining associated with the surface (paths [4] and [5]).

Depending on the extent of the hydrolysis, the concentration of these newly formed protonated surface hydroxyl groups may be quite significant, compensating in an analogous way the number of hydroxyl groups consumed during deposition of chromium species and, consequently, providing an additional number of sites for deposition of the V species. In such a case the protonated surface hydroxyl groups available for deposition of $V_xO_y^{z-}$ species following the prior deposition of a small loading of Cr (2 mol%) would be almost the same as that before the chromium deposition, thus ensuring the highest dispersion of vanadate species.

This deposition mechanism is in accordance with the XPS result presented in Figs. 7 and 8. In fact, in this sample, the dispersion of the chromia phase remains unaffected after deposition of the vanadia phase (see Fig. 7), indicating that the hydrolyzed monomeric chromium species remain associated with the titania surface during impregnation with vanadium. In addition, dispersion of the vanadium phase also remains unaffected by prior deposition of chromia (see Fig. 8), indicating that the concentration of the deposition sites for the $V_xO_y^{z-}$ species also remains unaffected by prior deposition of chromia, as suggested by the above mechanism.

According to the above deposition mechanism the total number of surface hydroxyl groups used in the $TiCr_2V_6$ catalyst for the deposition of both active phases could be greater than that of the other binary active phase-containing catalysts, as in those cases monomeric Cr^{6+} species have not been detected. This is in agreement with the higher surface coverage observed for this catalyst. This view is in excellent agreement with our XPS (Fig. 9) and DRS (Fig. 2) results, while it explains the homogeneity of this catalyst observed by AEM.

The deposition of V^{5+} species on sites adjacent to the isolated Cr^{6+} species might also favor the creation of Cr–O–V bridges during calcination of the catalyst, thus transforming the above units in nonisolated ones. This would explain perfectly the fact that after the deposition of vanadia an increase is observed in the concentration of octahedral nonterminal chromate units [as concluded from the analogous increase in the intensity of the LRM band in the range 870–1000 cm^{-1} (7)]. In our previous work (16) only isolated tetrahedral Cr^{6+} species were detected in the sample containing 2 mol% Cr. In contrast, the results of the present study show that the intensity of the bands in the above-mentioned spectral region takes its maximum value in the sample containing 2 mol% Cr ($TiCr_2V_6$), thus confirming an interaction between the two supported phases. This interaction transforms the isolated Cr^{6+} species, existing in the $TiCr_2V_0$ precursor sample, into nonterminal chromate species in the $TiCr_2V_6$ catalyst. A result of this interaction may also be the new Raman peak at 971 cm^{-1}, which appeared in the spectrum of this sample. This peak does not appear in either the spectrum of $TiCr_2V_0$ or the spectrum of $TiCr_0V_6$ (see Fig. 3). It should be noted that the relative intensity of the Raman peak at 971 cm^{-1} diminishes when the sample is irradiated with "high laser intensity." Taking into account the crystallization effect of "high laser intensity" on the two supported phases (7, 16, 32) one can conclude that, indeed, the species responsible for the above peak are well dispersed on the titania surface, in accordance with the proposed deposition mechanism.

The increase observed in the intensity of the Raman signal of the $TiCr_2V_6$ sample in the range 870–1000 cm^{-1} might also be attributed to the influence of the chromia phase, which is acidic, on the structure of the vanadia phase. According to Deo and Wachs (31), acidic additives, like WO_3, Nb_2O_5, and P_2O_5, create more polymerized and six-coordinated vanadium oxide structures in vanadia–titania catalysts. This is reflected by an upward shift of the corresponding Raman band from ~950 to 970–980 cm^{-1}. However, as can be seen in Fig. 3, even in the spectrum of a vanadia–titania sample containing 8 mol% V, the intensity of the corresponding Raman band is too low to explain the increase observed in the case of the $TiCr_2V_6$ sample.

On this point, it should be also stressed that the TPR curve of the $TiCr_2V_6$ catalyst showing a rather symmetrical reduction peak at 500°C corroborates the view that a new predominant Cr–O–V phase is formed on the surface of this catalyst.

In the case of the $TiCr_4V_4$ catalyst, the majority of the Cr^{6+} species formed in the first impregnation step are oligomeric species (16). According to the proposed deposition mechanism some of these species are completely hydrolyzed, some partially hydrolyzed, and some not hydrolyzed during the second impregnation step. The completely hydrolyzed oligomeric species is expected to

precipitate on the support surface after removal of water and result in a lower dispersion of the chromium phase than measured in the precursor solid ($TiCr_4V_0$). This is confirmed by the XPS results presented in Fig. 7. On the other hand, because of the small number of protonated hydroxyl groups per chromate unit created due to the partially hydrolyzed chromium oligomeric species and the occupation of some of the existing surface hydroxyl groups by the partially hydrolyzed and nonhydrolyzed chromium species, the dispersion of the vanadium phase is expected to be lower than that measured in the $TiCr_0V_4$ sample. This is in agreement with the XPS results presented in Fig. 8. However, because of the deposition of V^{5+} species on surface hydroxyl groups—unoccupied by chromium species and that created by the partial hydrolysis of chromium species—the total coverage of the support surface in the $TiCr_4V_4$ catalyst might be higher than that of binary samples with the same total loading but lower than that achieved in the $TiCr_2V_6$ catalyst, in agreement with XPS and DRS results.

In the $TiCr_6V_0$ sample, the precursor of $TiCr_6V_2$, the main fraction of chromia is badly dispersed on the support surface, forming agglomerates or crystallites (16). Some of these badly dispersed chromium species are expected to be partially hydrolyzed during the second impregnation step. Thus no change in the dispersion of the chromium phase is observed after the deposition of vanadia (Fig. 7). In this sample the chromium loading is high and corresponds to the maximum surface coverage of titania by chromium (see Fig. 7). Thus, the deposition sites remaining unoccupied by the chromium species are expected to be quite few. This explains why, although the vanadium loading in this case is low, the vanadia dispersion is lower than that measured in the $TiCr_0V_2$ sample (Fig. 8). As vanadium species are deposited on surface sites that are unoccupied by the chromium phase and on sites created by the partial hydrolysis of the chromium surface species, the coverage of the support surface achieved in the $TiCr_6V_2$ catalyst is higher than that of the binary $TiCr_8V_0$ and $TiCr_0V_8$ samples and lower than that of the other ternary ones (see Figs. 2 and 9).

The deposition mechanism proposed above, although a tentative one, can explain very well the differences in the physicochemical characteristics of the ternary catalysts.

Catalytic Performance of $TiCr_xV_y$ Catalysts

The results obtained have shown that, at low reaction temperature (250°C), where the reduction of NO by NH_3 is the predominant reaction of this process, the specific activity of the catalysts studied increases as the V/Cr atomic ratio increases. This means that V species are more active than Cr species for the above reaction. However, the favorable action of Cr species on the global activity of the ternary catalysts can be seen even at this low reaction temperature. Indeed, as has already been discussed, Cr species have a stabilizing effect on the surface area of the prepared catalysts. This fact seems to have a positive influence on the global activity of $TiCr_2V_6$ catalyst, rendering this catalyst more active than $TiCr_0V_8$. The $TiCr_2V_6$ catalyst proved to be the most active catalyst of the series at reaction temperatures up to 350°C. We need to note that this catalyst has the highest surface area, exhibits maximum surface coverage of the support by the supported phases, and consequently has the maximum dispersion of the active phases and the most extended interactions between the active phases and the carrier based on AEM, XPS, and DRS results. However, even in the above-mentioned region of reaction temperatures, the global activity order of the catalysts changed with temperature. This means that the above-mentioned physicochemical parameters are not the only factors determining the catalytic performance of the prepared samples.

At higher reaction temperatures the ternary samples proved to be more effective than the corresponding binary ones. To a first approximation this could be attributed to better geometrical characteristics (dispersion, surface area, supported phase–support interactions) of the supported phases, observed in the cases of the ternary samples, compared with those of the corresponding binary ones. However, inspection of Fig. 11 reveals that the order established taking into account the percentage NO conversion values, measured at these high reaction temperatures (>350°C), depends both on the composition of the catalysts and on reaction temperature.

The catalytic behavior discussed above implies that changes in the composition of the prepared catalysts affect not only the geometrical characteristics of the supported phases but also the kind and concentration of active sites formed on their surfaces, probably by changing the structure of supported species. It seems that these sites are responsible for the acceleration of the various reactions taking place during the SCR process and are activated at different reaction temperatures. The above considerations can also explain the dependence of NH_3 consumption on both composition and reaction temperature. In fact, a comparison of the % x_{NO} and % x_{NH3} values (Figs. 11 and 12) reveals that NH_3 is consumed in excess of NO converted as the Cr content of the catalyts and the reaction temperature increase. As a result of this behavior total consumption of NH_3 is observed at 350°C over the $TiCr_8V_0$ catalyst, at 400°C over the $TiCr_6V_2$ catalyst, and at 450°C over the remaining catalysts studied ($TiCr_4V_4$, $TiCr_2V_6$, and $TiCr_0V_8$). These observations verify that other side reactions involving NH_3 but not NO, like [8], [9], and [10], also take place at reaction temperatures higher than 350°C:

$$4NH_3 + 3O_2 \rightarrow 2N_2 + 6H_2O, \quad [8]$$

$$2NH_3 + 2O_2 \rightarrow N_2O + 3H_2O, \quad [9]$$

$$4NH_3 + 5O_2 \rightarrow 4NO + 6H_2O. \quad [10]$$

Taking into account the above-discussed complexity of the SCR process, we think that the yield toward N_2, which is the desired product of the process, should be considered the most important criterion for evaluation of the catalysts studied.

The results presented in Fig. 13 show that the yield of N_2 depends on both the composition of the catalysts and the reaction temperature. At temperatures up to 350°C, where reaction [3] is expected to be predominant, the vanadium-rich samples ($TiCr_0V_8$ and $TiCr_2V_6$) give higher yields of N_2, in accordance with the fact that vanadia phase is more active for this reaction than chromia phase, as has been concluded from the specific activities presented in Table 2. However, the favorable action of the chromia phase is evident even at these low reaction temperatures, rendering the $TiCr_2V_6$ catalyst more selective than the $TiCr_0V_8$ catalyst. The favorable action produced by the coexistence of the two supported phases on the activity and selectivity of these catalysts proves that a synergy is developed between the two phases. This synergy is more pronounced at even higher reaction temperatures where the side reactions [8]–[10] are also accelerated. Indeed at temperatures higher than 350°C not only the $TiCr_2V_6$ catalyst but all the ternary samples proved to be more effective, exhibiting higher selectivity to reaction [3] than the corresponding binary ones. However, the fact that the $TiCr_2V_6$ catalyst proved to be the best catalyst of the series means that the above mentioned synergy is maximized in the corresponding composition.

The above-discussed catalytic behavior of the $TiCr_xV_y$ catalysts for the SCR of NO by NH_3 in excess O_2, combined with the results of the physiochemical characterization of the corresponding samples, suggest that the synergy observed should be related to the concentration of Cr–O–V interaction species, created by the decoration of isolated Cr species with well-dispersed V species. In accordance with what we have already discussed in a previous work (16), the concentration of isolated Cr^{6+} species on the precursor solids ($TiCr_xV_0$) decreases as the Cr content increases. This is expected to bring about a corresponding decrease in the concentration of the above-mentioned Cr–O–V interaction species, in agreement with the physicochemical characterization results, discussed in a previous section of this work.

CONCLUSIONS

The most important conclusions drawn from the present study may be summarized as follows:

1. A synergy is detected between chromia and vanadia phases supported on anatase surface for the SCR of NO by NH_3, in excess O_2. This synergy is more pronounced at high reaction temperatures.

2. The synergy observed seems to be due to the creation of Cr–O–V interaction species between the isolated Cr^{6+} species and the well-dispersed V^{5+} species.

3. The existence of chromia phase on the titania support stabilizes the texture of the final $TiCr_xV_y$ catalysts against changes provoked by deposition of the vanadia phase.

ACKNOWLEDGMENTS

Financial support by the European Union (Project Environment, Contract EV5V-CT92-0234) is gratefully acknowledged. Thanks are also due Professor B. Delmon for premission to carry out a part of the experimental work (XPS, AEM) in the laboratory of the Unité de Catalyse et Chimie des Materiaux Divisés, Université Catholique de Louvain, Louvain-la-Neuve, Belgium.

REFERENCES

1. Curry-Hyde, E., and Baiker, A., *Ind. Eng. Chem. Prod. Res. Dev.* **29**, 1985 (1990).
2. Curry-Hyde, H. E., Musch, H., and Baiker, A., *Appl. Catal.* **65**, 211 (1990).
3. Curry-Hyde, H. E., and Baiker, A., *Appl. Catal.* **90**, 183 (1992).
4. Schraml-Marth, M., Wokaun, A., Curry-Hyde, H. E., and Baiker, A., *J. Catal.* **133**, 415 (1992).
5. Köhler, K., Schläpfer, C. W., von Zelewsky, A., Nickl, J., Engweiler, J., and Baiker, A., *J. Catal.* **143**, 201 (1993).
6. Engweiler, J., Nickl, J., Baiker, A., Köhler, K., Schläpfer, C. W., and von Zelewsky, A., *J. Catal.* **145**, 141 (1994).
7. Scharf, U., Schneider, H., Baiker, A., and Wokaun, A., *J. Catal.* **145**, 464 (1994).
8. Schneider, H., Scharf, U., Wokaun, A., and Baiker, A., *J. Catal.* **147**, 545 (1994).
9. Duffy, B. L., Curry-Hyde, H. E., Cant, N. W., and Nelson, P. F., *Appl. Catal. B* **5**, 133 (1994).
10. Duffy, B. L., Curry-Hyde, H. E., Cant, N. W., and Nelson, P. F., *J. Catal.* **149**, 11 (1994).
11. Köhler, K., Maciejewski, M., Schneider, H., and Baiker, A., *J. Catal.* **157**, 301 (1995).
12. Schneider, H., Maciejewski, M., Köhler, K., Wokaum, A., and Baiker, A., *J. Catal.* **157**, 312 (1995).
13. Duffy, B. L., Curry-Hyde, H. E., Cant, N. W., and Nelson, P. F., *J. Catal.* **154**, 107 (1995).
14. Bosch, H., and Janssen, F., *Catal. Today* **2**, 369 (1988).
15. Nakatsuji, T., and Miyamoto, A., *Catal. Today* **10**, 21 (1991).
16. Fountzoula, Ch., Matralis, H. K., Papadopoulou, Ch., Voyiatzis, G. A., and Kordulis, Ch., *J. Catal.* **177**, 391 (1997).
17. Wong, W. C., and Nobe, K., *Ind. Eng. Chem. Prod. Res. Dev.* **25**, 179 (1986).
18. Grange, P., *Catal. Rev. Sci. Eng.* **21**, 1 (1980).
19. Spanos, N., Matralis, H. K., Kordulis, Ch., and Lycourghiotis, A., *J. Catal.* **136**, 432 (1992).
20. del Arco, M., Holgado, M. J., Martin, C., and Rives, V., *Spectrosc. Lett.* **20**, 201 (1987).
21. Ramis, G., Busca, G., Cristiani, C., Lietti, L., Forzatti, P., and Bregani, F., *Langmuir* **8**, 1744 (1992).
22. Del Arco, M., Martin, C., Rives, V., Sanchez-Escribano, V., Ramis, G., Busca, G., Lorenzelli, V., and Malet, P., *J. Chem. Soc. Faraday Trans.* **89**, 1071 (1993).
23. Inomata, M., Mori, K., Ui, T., Miyamoto, A., and Murakami, Y., *J. Phys. Chem.* **87**, 754 (1983).
24. Malet, P., Munoz-Paez, A., Martin, C., and Rives, V., *J. Catal.* **134**, 47 (1992).
25. Schoonheydt, R. A., *in* "Characterization of Heterogeneous Catalysts" (F. Delanay, Ed.), Ch. 4. Dekker, New York/Basel, 1984.
26. Hardcastle, F. D., and Wachs, I. E., *J. Mol. Catal.* **46**, 173 (1988).

27. Nobbenhuis, M. G., Baiker, A., Barnickel, P., and Wokaun, A., *Appl. Catal.* **85**, 157 (1992).
28. Chan, S. S., Wachs, I. E., Murrell, L. L., Wang, L., and Hall, W. K., *J. Phys. Chem*. **88**, 5831 (1984).
29. Machej, T., Haber, J., Turek, A. M., and Wachs, I. E., *Appl. Catal.* **70**, 115 (1991).
30. Nickl, J., Dutoit, D., Baiker, A., Scharf, U., and Wokaun, A., *Appl. Catal.* **98**, 173 (1993).
31. Deo, G., and Wachs, I. E., *J. Catal.* **146**, 335 (1994).
32. Cristiani, C., Forzatti, P., and Busca, G., *J. Catal.* **116**, 586 (1989).
33. Wagner, C. D., Riggs, W. M., Davis, L. E., Moulder, J. F., and Muilenberg, G. E., "Handbook of X-Ray Photoelectron Spectroscopy: A Reference Book of Standard Data for Use in X-Ray Photoelectron Spectroscopy." Physical Electronics Division, Perkin-Elmer Corp., Eden Prairie, MN, 1979.
34. Haber, J., Machej, T., and Czeppe, T., *Surf. Sci.* **151**, 301 (1985).
35. Centi, G., Pinelli, D., Trifiro, F., Ghoussoub, D., Guelton, M., and Gengembre, L., *J. Catal.* **130**, 238 (1991).
36. Odriozola, J. A., Soria, J., Somorjai, G. A., Heinemann, H., Garcia de la Banda, J. F., Lopez Granados, M., and Conesa, J. C., *J. Phys. Chem*. **95**, 240 (1991).
37. Nickl, J., Schlogl, R., Baiker, A., Knozinger, H., and Ertl, G., *Catal. Lett.* **3**, 379 (1989).
38. Andersson, S. L. T., *Catal. Lett.*, 351 (1990).
39. Centi, G., Giamello, E., Pinelli, D., and Trifiro, F., *J. Catal.* **130**, 220 (1991).
40. Ciambelli, P., Bagnasco, G., Lisi, L., Turco, M., Chiarello, G., Musci, M., Notaro, M., Robba, D., and Ghetti, P., *Appl. Catal. B* **1**, 61 (1992).
41. Roozeboom, F., Mittelmeljer-Hazeleger, M. C., Moulijn, J. A., Medema, J., de Beer, V. H. J., and Gellings, P. J., *J. Phys. Chem*. **84**, 2738 (1980).
42. Wachs, I. E., Saleh, R. Y., Chan, S. S., and Chersich, C. C., *Appl. Catal.* **15**, 339 (1985).
43. Bosch, H., Janssen, J. J. G., van den Kerkhof, F. M. G., Oldenziel, J. van Ommen, J. C., and Ross, J. R. H., *Appl. Catal.* **25**, 239 (1986).
44. Georgiadou, I., Slavov, S., Papadopoulou, Ch., Matralis, H. K., and Kordulis, Ch., *Bull. Soc. Chim. Belg.* **104**, 143 (1995).
45. Matralis, H. K., Papadopoulou, Ch., Kordulis, Ch., Aguilar-Elguezabal, A., and Cortes-Corberan, V., *Appl. Catal.* **125**, 365 (1995).
46. Baiker, A., Dollenmaier, P., Glinski, M., and Keller, A., *Appl. Catal.* **37**, 315 (1987).
47. Quaranta, N. E., Cortes Corberan, V., and Fierro, J. L. G., *Stud. Surf. Sci. Catal.* **72**, 147 (1992).
48. Ciambelli, P., Lisi, L., Russo, G., and Volta, J. C., *Appl. Catal.* **151**, 226 (1995).
49. Turco, M., Lisi, L., Pirone, R., and Ciambelli, P., *Appl. Catal. B* **3**, 133 (1994).
50. Odenbrand, C. U. I., Gabrielsson, P. L. T., Brandin, J. G. M., and Andersson, L. A. H., *Appl. Catal.* **78**, 109 (1991).
51. Del Arco, M., Holgado, M. J., Martin, C., and Rives, V., *J. Catal.* **99**, 19 (1986).
52. Spanos, N., Slavov, S., Kordulis, Ch., and Lycourghiotis, A., *Colloids Surf.* **97**, 109 (1995).
53. Bourikas, K., Spanos, N., and Lycourghiotis, A., *Langmuir* **13**, 435 (1997).